PITCH BOUNCE OSCILLATION OF A LONG AND HEAVY TANDEM-SUSPENDED HELICOPTER UNDERSLUNG LOAD

T. W. G. de Laat[1], M. D. Pavel[2], and N. A. Heerink[1]

[1] Netherlands Defence Academy, Faculty Military Sciences
Het nieuwe Diep 8, 1780 CA Den Helder, The Netherlands
e-mail: twg.d.laat@nlda.nl

[2] Delft University of Technology, Department of Aerospace Engineering
Kluyverweg 1, 2629 HS Delft, The Netherlands
e-mail: m.d.pavel@tudelft.nl

Key words: External load, underslung load, tandem suspension, vertical bounce, pitch oscillation, pitch bounce

Abstract. In this paper the pitch bounce oscillation of a tandem-suspended long and heavy underslung load is investigated. It is compared with a case of violent pitch oscillation experienced in flight with a Chinook helicopter with such an underslung load. It is concluded that it is very likely that in that case the helicopter plus load were excited close to the pitch bounce natural frequency leading to a resonant condition. The paper hypothesized that the motion was negatively affected by the rotor downwash or more specifically the tip vortices of the rotor blades and that the system had not enough aerodynamic damping.

1. INTRODUCTION

A Chinook helicopter of the Royal Netherlands Air Force experienced a violent pitch oscillation during an external load operation with a large open tower construction suspended in a tandem cargo hook configuration, see Fig. 1. As the helicopter and underslung load were experiencing pitch oscillations, which were in opposite direction, so in anti-phase, it was presumed to be a potential elasticity matter, such as for a single suspension would be called "vertical bounce", see Gabel & Wilson [2]. Typically, the vertical bouncing phenomenon is a dynamic resonance condition which occurs when the natural frequency of the helicopter with its sling load, as a mass-spring-system, is close to the once per revolution frequency of the helicopter rotor. This motion would normally dampen, but might be divergent in case of out-of-phase steering input, see Gabel & Wilson [2]: "A disturbance in the system can induce a vertical vibration at the system natural frequency which under normal circumstances would damp rapidly. However, the presence of the pilot and his thrust lever control can add another element to the system which can lead to a divergent oscillation". In vertical bounce, motion coupling can be accomplished by the pilot's arm and depends then on his arm stiffness and the force that is induced through his body motion to the collective lever motion. That is why vertical bouncing can be associated to a pilot induced oscillation problem as the pilot is unconsciously exciting divergent vehicle oscillations by applying control inputs that are in the wrong direction or have phase lag.

The tandem cargo hook suspension is an interesting application as it can easily counter the yaw instability (e.g. Prabhakar [3]) of an underslung load, but it might in this case have resulted in another type of instability, which could be called "pitch bounce". In this

Figure 1. Picture of the tandem-suspension external load under tandem-rotor helicopter.

paper the dynamics of such a pitch bounce oscillation of a tandem-suspended long and heavy load under a helicopter is treated.

2. EQUATIONS OF MOTION

We define the equations of motion in the horizontal earth-fixed axis system through the centre of gravity of the helicopter, with the x axis (horizontal reference line, hrl) positive to the rear of the helicopter and the z axis in the direction of the gravity (weight W), see Fig. 2. From Fig. 2 we have the coordinates of the points 1, 2, 3 and 4 for the equilibrium of the helicopter in hovering flight:

$$\begin{array}{ll} (x_{1_0}, z_{1_0}) = (-a_1, b_1), & (x_{2_0}, z_{2_0}) = (a_2, b_2), \\ (x_{3_0}, z_{3_0}) = (-d - a_3, h - b_3), & (x_{4_0}, z_{4_0}) = (-d + a_4, h - b_4). \end{array} \tag{1}$$

The motion under investigation was predominantly a pitching motion of helicopter and load, furthermore the vertical displacement of helicopter and load plays a role, we assume four degrees of freedom (4 DOF) θ_h, θ_l, z_h, and z_l, corresponding to respectively helicopter pitch attitude, load pitch attitude, helicopter vertical position and load vertical position w.r.t. the defined system of coordinates. In Fig. 2 the fuselage reference line (frl) of the helicopter is drawn in the equilibrium position and after disturbance θ_h of the attitude (frl'). We consider small disturbances $(\theta_h, \theta_l, z_h, z_l)$ from the equilibrium position $(\theta_{h_0}, \theta_{l_0}, z_{h_0}, z_{l_0})$ and after linearization with $\cos\theta \approx 1$ and $\sin\theta \approx \theta$, we obtain

$$\begin{array}{l} (x_1, z_1) = (-a_1 - b_1\theta_h, b_1 - a_1\theta_h + z_h), \\ (x_2, z_2) = (a_2 - b_2\theta_h, b_2 + a_2\theta_h + z_h), \\ (x_3, z_3) = (-d - a_3 + b_3\theta_l, h - b_3 - a_3\theta_l + z_l), \\ (x_4, z_4) = (-d + a_4 + b_4\theta_l, h - b_4 + a_4\theta_l + z_l). \end{array} \tag{2}$$

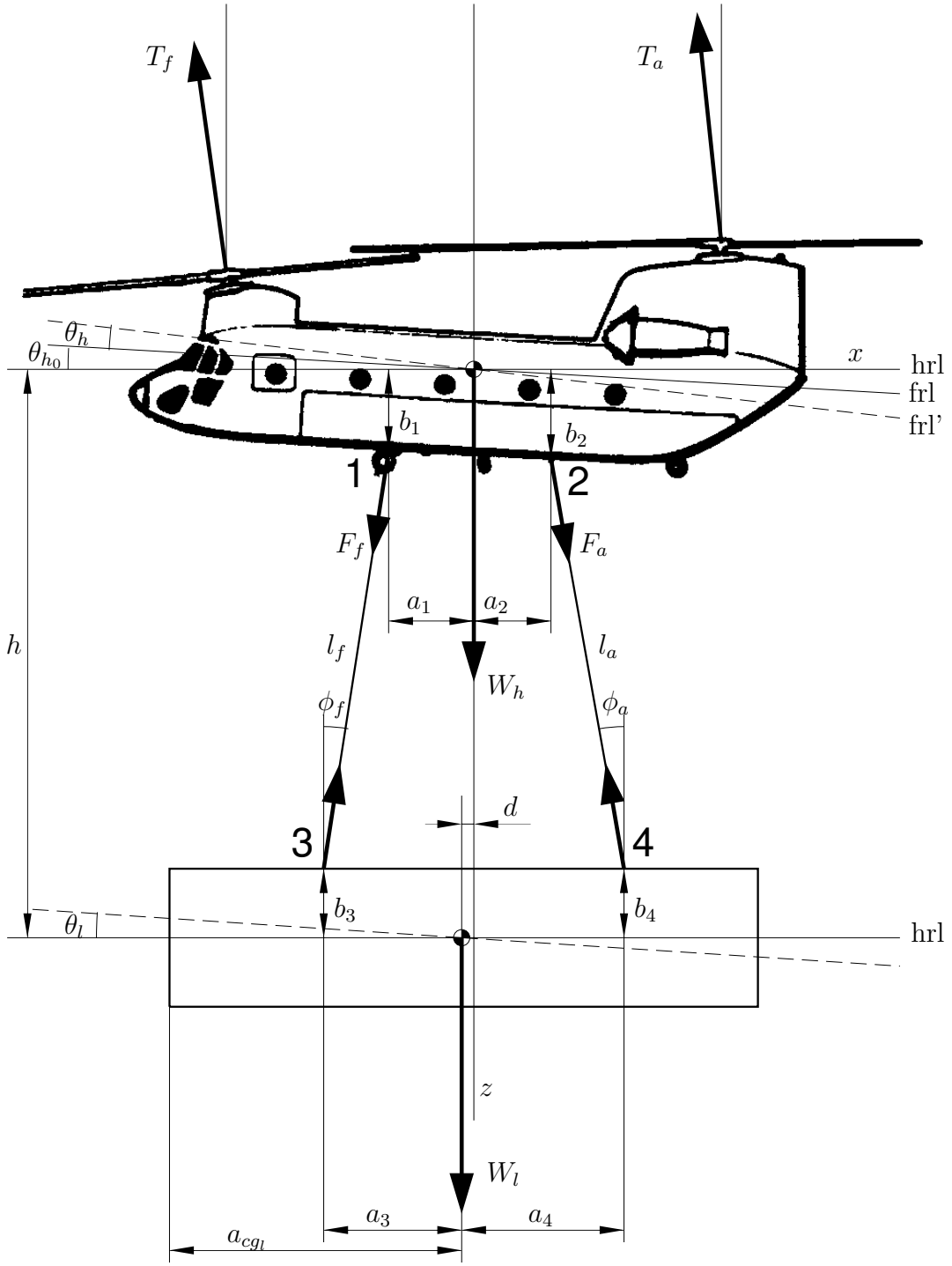

Figure 2. Tandem-suspension external load under tandem-rotor helicopter.

As the weights of helicopter and load are heavy and the external load is an open construction, the damping which would be the result of the aerodynamic force is omitted. If we consider the disturbances from the equilibrium, the equations of motion are:

$$\begin{aligned}
I_{y_h}\ddot{\theta}_h &= k_f\Delta l_f\left(-a_1\cos\phi_f + b_1\sin\phi_f\right) + k_a\Delta l_a\left(a_2\cos\phi_a - b_2\sin\phi_a\right),\\
I_{y_l}\ddot{\theta}_l &= k_f\Delta l_f\left(a_3\cos\phi_f + b_3\sin\phi_f\right) - k_a\Delta l_a\left(a_4\cos\phi_a + b_4\sin\phi_a\right),\\
m_h\ddot{z}_h &= k_f\Delta l_f + k_a\Delta l_a,\\
m_l\ddot{z}_l &= -k_f\Delta l_f - k_a\Delta l_a,
\end{aligned} \tag{3}$$

in which k_f and k_a are the spring constants of the forward and aft slings, respectively. The elongations of the forward and aft slings relative to the equilibrium position are defined by

$$\Delta l_f = l_f - l_{f_0} \quad \text{and} \quad \Delta l_a = l_a - l_{a_0}. \tag{4}$$

They are calculated from Eqs. (1) and (2), by

$$\begin{array}{ll} l_{f_0} = \sqrt{(x_{1_0} - x_{3_0})^2 + (z_{1_0} - z_{3_0})^2}, & l_{a_0} = \sqrt{(x_{2_0} - x_{4_0})^2 + (z_{2_0} - z_{4_0})^2}, \\ l_f = \sqrt{(x_1 - x_3)^2 + (z_1 - z_3)^2}, & l_a = \sqrt{(x_2 - x_4)^2 + (z_2 - z_4)^2}. \end{array} \tag{5}$$

Substitution of Eqs. (5) with (1) and (2) into (4) and approximation to first order of θ_h, θ_l, z_h, and, z_l, and furthermore using the Taylor series for the square root ($\sqrt{1+\theta} \approx 1 + \frac{1}{2}\theta + O(\theta^2)$), yields

$$\begin{aligned} \Delta l_f &= (c_1\theta_h + c_2\theta_l)/l_{f_0} + c_3(z_l - z_h) + O(\theta^2), \\ \Delta l_a &= (c_4\theta_h + c_5\theta_l)/l_{a_0} + c_6(z_l - z_h) + O(\theta^2), \end{aligned} \tag{6}$$

with

$$\begin{array}{lll} c_1 = -a_1b_3 + a_1h - a_3b_1 - b_1d, & c_2 = a_1b_3 + a_3b_1 - a_3h - b_3d, & c_3 = h - b_1 - b_3, \\ c_4 = a_2b_4 - a_2h + a_4b_2 - b_2d, & c_5 = -a_2b_4 - a_4b_2 + a_4h - b_4d, & c_6 = h - b_2 - b_4. \end{array} \tag{7}$$

Substitution of (6) into (3) yields with $\cos\phi_f \approx 1$, $\cos\phi_a \approx 1$, $\sin\phi_f \approx \phi_{f_0}$, and $\sin\phi_a \approx \phi_{a_0}$:

$$\begin{bmatrix} \ddot{\theta}_h \\ \ddot{\theta}_l \\ \ddot{z}_h \\ \ddot{z}_l \end{bmatrix} = \begin{bmatrix} e_1c_1 + e_2c_4 & e_1c_2 + e_2c_5 & -e_1c_3 - e_2c_6 & e_1c_3 + e_2c_6 \\ e_3c_1 - e_4c_4 & e_3c_2 - e_4c_5 & -e_3c_3 + e_4c_6 & e_3c_3 - e_4c_6 \\ e_3c_1 + e_6c_4 & e_5c_2 + e_5c_5 & -e_5c_3 - e_6c_6 & e_5c_3 + e_6c_6 \\ -e_3c_1 - e_6c_4 & -e_5c_2 - e_5c_5 & e_5c_3 + e_6c_6 & -e_5c_3 - e_6c_6 \end{bmatrix} \begin{bmatrix} \theta_h \\ \theta_l \\ z_h \\ z_l \end{bmatrix} + O\left(\theta^2\right), \tag{8}$$

with

$$\begin{array}{ll} e_1 = (-a_1 + b_1\phi_{f_0})\, k_f/(l_{f_0}I_{y_h}), & e_2 = (a_2 - b_2\phi_{a_0})\, k_a/(l_{a_0}I_{y_h}), \\ e_3 = (a_3 + b_3\phi_{f_0})\, k_f/(l_{f_0}I_{y_l}), & e_4 = (a_4 + b_4\phi_{a_0})\, k_a/(l_{a_0}I_{y_l}), \\ e_5 = k_f/l_{f_0}, & e_6 = k_a/l_{a_0}. \end{array} \tag{9}$$

These equations of motion can furthermore be written as a system of eight first-order differential equations, with the introduction of $q_h \equiv \dot{\theta}_h$, $q_l \equiv \dot{\theta}_l$, $w_h \equiv \dot{w}_h$, and $w_l \equiv \dot{w}_l$:

$$\begin{bmatrix} \dot{\theta}_h \\ \dot{q}_h \\ \dot{\theta}_l \\ \dot{q}_l \\ \dot{z}_h \\ \dot{w}_h \\ \dot{z}_l \\ \dot{w}_l \end{bmatrix} = \begin{bmatrix} 0 & 1 & 0 & 0 & 0 & 0 & 0 & 0 \\ A_{11} & 0 & A_{12} & 0 & -A_{13} & 0 & A_{13} & 0 \\ 0 & 0 & 0 & 1 & 0 & 0 & 0 & 0 \\ A_{21} & 0 & A_{22} & 0 & -A_{23} & 0 & A_{23} & 0 \\ 0 & 0 & 0 & 0 & 0 & 1 & 0 & 0 \\ A_{31} & 0 & A_{32} & 0 & -A_{33} & 0 & A_{33} & 0 \\ 0 & 0 & 0 & 0 & 0 & 0 & 0 & 1 \\ -A_{31}\frac{m_h}{m_l} & 0 & -A_{32}\frac{m_h}{m_l} & 0 & A_{33}\frac{m_h}{m_l} & 0 & -A_{33}\frac{m_h}{m_l} & 0 \end{bmatrix} \begin{bmatrix} \theta_h \\ q_h \\ \theta_l \\ q_l \\ z_h \\ w_h \\ z_l \\ w_l \end{bmatrix} + O\left(\theta^2\right), \tag{10}$$

with

$$\begin{array}{lll} A_{11} = e_1c_1 + e_2c_4, & A_{12} = e_1c_2 + e_2c_5, & A_{13} = e_1c_3 + e_2c_6, \\ A_{21} = e_3c_1 - e_4c_4, & A_{22} = e_3c_2 - e_4c_5, & A_{23} = e_3c_3 - e_4c_6, \\ A_{31} = (e_5c_1 + e_6c_4)/m_h, & A_{32} = (e_5c_2 + e_6c_5)/m_h, & A_{33} = (e_5c_3 + e_6c_6)/m_h. \end{array}$$

This system of first-order differential equations can be solved using the method of eigenvalues. The equilibrium is stable when the real parts of both eigenvalues are negative, implying that if the equilibrium is disturbed, the displacement will tend to zero. As we have not included the aerodynamic damping, we have a conservative system.

3. EVALUATATION OF THE PITCHING MOTION OF THE SPECIFIC SYSTEM

3.1 Flight with an open construction tower

The underslung load with which the violent pitching oscillation was experienced, was an open construction steel tower with suspension as in Figs. 1 and 2. For the fore and aft suspension five-meter extension strops were used in combination with two-legged slings to obtain two inverted-Y suspensions. The load was rigged with consideration of a 3 deg attitude of the Chinook, so the front extension legs were made 20 cm longer than the aft sling legs. Furthermore a slack redundant sling, see Fig. 1 (but not shown in Fig. 2), was attached to the load and the centre cargo hook. The centre of gravity in the fuselage reference system of the Chinook CH-47D of the Royal Netherlands Air Force, was at fuselage station 326 inch and at 35.4 inch waterline, with the front and aft cargo hooks, respectively, at fuselage stations 249 and 409 inch. The data is given in Table 1.

helicopter			load			slings	
a_1=	2.1	m	a_3=	3.4	m	k_f= 1.2×10^6	N/m
a_2=	2.0	m	a_4=	4.0	m	k_a= 1.2×10^6	N/m
b_1=	2.1	m	b_3=	1.7	m	l_{f_0}= 11.3	m
b_2=	2.3	m	b_4=	1.7	m	l_{a_0}= 11.1	m
			h =	15.0	m	ϕ_{f_0}=8.2	deg
			d =	0.3	m	ϕ_{a_0}=8.8	deg
θ_{h_0} =	3	deg	θ_{l_0} =	0	deg		
z_{h_0} =	0	m	z_{l_0} =	h	m		
m_h=	13.5×10^3	kg	m_l=	9.3×10^3	kg		
I_{y_h}=	2.74×10^5	kgm^2	I_{y_l}=	1.72×10^5	kgm^2		
			a_{cg_l}=	7.2	m		
			length=	14.5	m		
			width=	3.4	m		
			height=	3.4	m		

Table 1. Data of the specific tandem load under Chinook CH-47D.

The spring constant of the nylon slings, see Table 1, are determined from data of the manufacturer of the extension strops. The spring constants of the two-legged slings were not available and were assumed to have the same elasticity as the extension strops. The cables appear to be very stiff in comparison to data used in studies of Cheng *et al.* [1], who used 16.4 to 20 kN/m and Sheldon [4], who used 29.3 and 73.2 kN/m.

3.2 Evaluation of the video recording

During the flight the airspeed remained less than 40 kts and the pitch oscillations were repeatedly experienced. The pitch oscillation became severe during the deceleration and landing. Some parts of the flight were recorded with a hand-held videocamera. Pictures from that recording were used to estimate the frequency of the motion. A few seconds of video of the vertical oscillation of the pilot in the cockpit, see Fig. 3(a), and some more seconds of the helicopter with load during the landing, see Fig. 3(b), were available. The video images were available at a rate of 25 frames per second. The video recording

(a) Inside the helicopter, distance between helmet knob and upper windshield edge.

(b) Distance between helicopter and load.

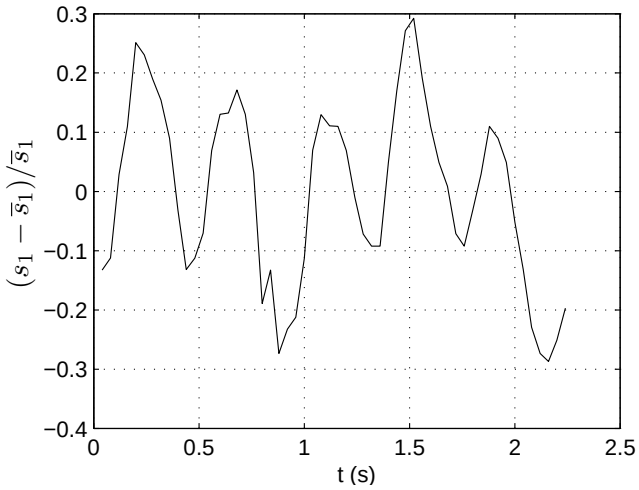

(c) Distance of helmet knob to windshield edge.

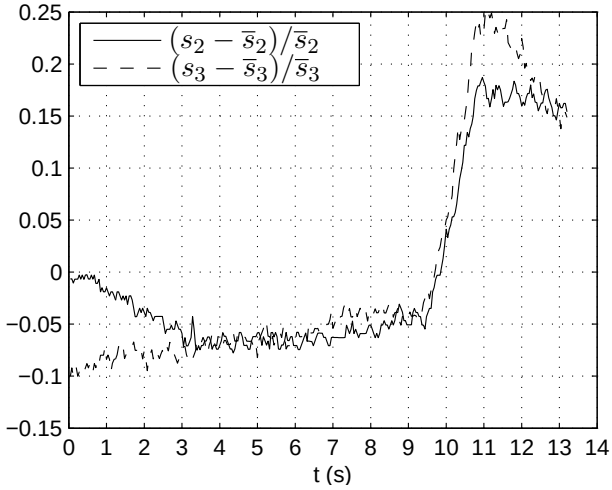

(d) Distance between helicopter and load.

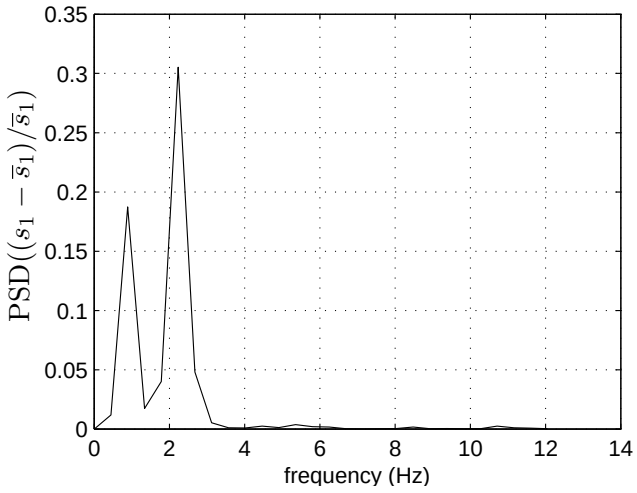

(e) Power spectral density (PSD) of $(s_1 - \overline{s}_1)/\overline{s}_1$.

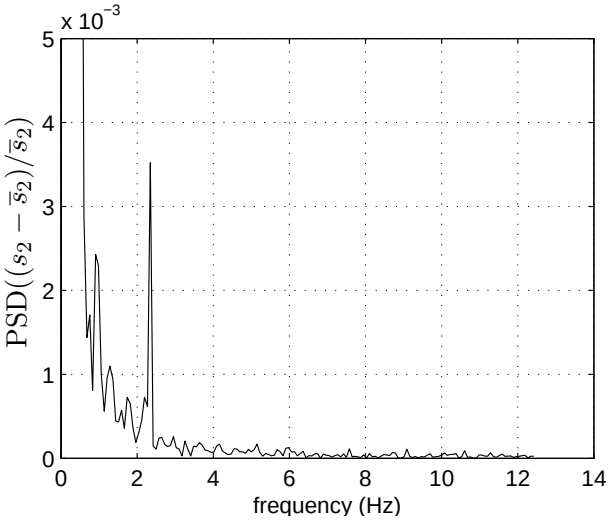

(f) Power spectral density (PSD) of $(s_2 - \overline{s}_2)/\overline{s}_2$.

Figure 3. Measured motion from the video images.

was decomposed in separate images to evaluate the motion. The separate pictures show double images of the rotor blades, as can be seen in Fig. 3(b). This is due to the camera

recording the pictures with a 50 Hz interlace technique in combination with the 25 frames per second recording rate of the videocamera. The oscillating motion was evaluated by measurement of:

1. the distance between helmet knob and upper edge of the windshield s_1, see arrow in Fig. 3(a),
2. the distance between front ends of the helicopter and load s_2, see forward arrow in Fig. 3(b),
3. the distance between aft ends of the helicopter and load s_3, see aft arrow in Fig. 3(b).

The resulting data in time is plotted, after subtraction of the mean value ($\overline{s}_1$, $\overline{s}_2$ and $\overline{s}_3$ respectively) and division by the respective mean value, in Figs. 3(c) and 3(d). There is some variation due to the relative motion of the helicopter with respect to the camera. Furthermore there is a major increase of the distance in Fig. 3(d) at $t \approx 10$ s, which is the result of zooming action of the camera lens. From the time traces, fast fourier transformations (FFT's) were made. The resulting power density plots of the data of Figs. 3(c) and 3(d) are given in Figs. 3(e) and 3(f), respectively. The frequency peaks of the observed motion correspond to 2.23 Hz in Fig. 3(e) and 2.35 Hz in Fig. 3(f).

3.3 Estimation of the natural frequencies

Using the linearized equations of motion (10) we can estimate the natural frequencies of this geometry. Substitution of the data from Table 1 into Eq. (10) and solving for the eigenvalues λ yields: $\lambda_{1,2} = \pm 15.48i$, $\lambda_{3,4} = \pm 20.82i$ and $\lambda_{5,6,7,8} = 0$. So, neglecting the aerodynamics, we have two periodic motions with the respective frequencies of $15.48/(2\pi) \approx 2.46$ Hz and $20.82/(2\pi) \approx 3.31$ Hz. The result of a simulation run of system (10) with the appropriate coefficients and with initial disturbance $\theta_l(t=0) = -0.01$ rad (-0.57 deg) and the other initial values equal to zero is given in Figs. 4(a) and 4(b). In Figs. 4(c) and 4(d) the results of a simulation run of the same system is shown for initial disturbance $z_l(t=0) = 0.05$ m with the other initial values equal to zero. In these figures the two natural frequencies are clearly shown. The natural frequency of 2.46 Hz is associated with a pitching oscillation of helicopter and load (θ_h, θ_l) which have opposite phase (anti-phase). The natural frequency of 3.31 Hz is related to the pure vertical bounce (z_h, z_l), which is also an anti-phase motion of helicopter and load. From these figures it is also clear that there is cross-coupling between these modes. This is the result of the asymmetry of the geometry $d \neq 0$, $a_1 \neq a_2$, $a_3 \neq a_4$ and $b_1 \neq b_2$.

From the equations of motion in z direction, which are the last two equations of (8) with $\theta_h = \theta_l = 0$, it can directly be derived that this pure vertical motion with the assumption $k_f = k_a = k$ has the vertical bounce frequency (see also, e.g. ref. [1]):

$$f_{vb} = \frac{1}{2\pi}\sqrt{2k\frac{m_h + m_l}{m_h m_l}}. \tag{11}$$

Substitution of the masses and stiffness constant from Table 1 yields f_{vb}=3.32 Hz, which is in agreement with the second natural frequency. This motion was not observed during the flight.

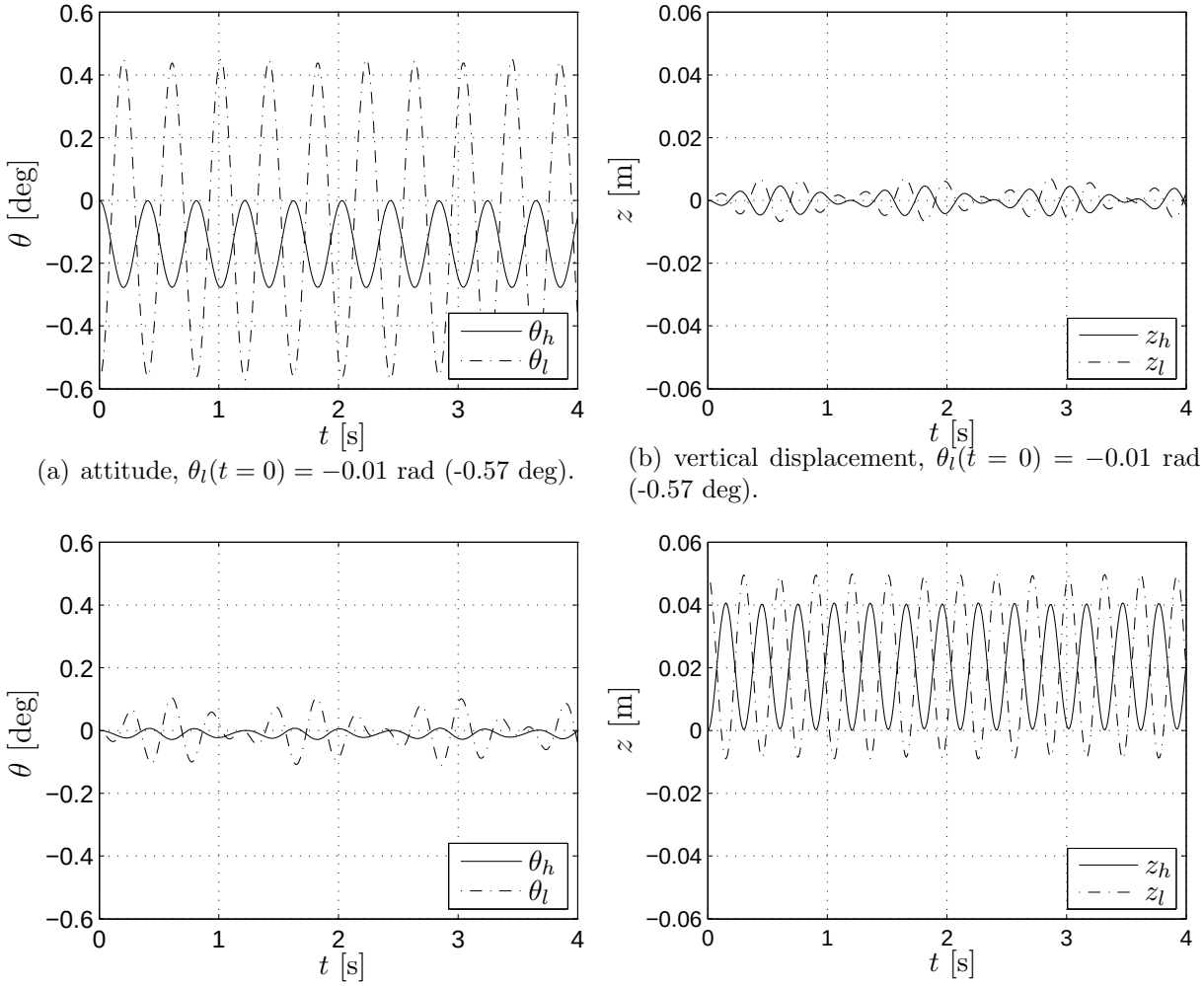

(a) attitude, $\theta_l(t=0) = -0.01$ rad (-0.57 deg).

(b) vertical displacement, $\theta_l(t=0) = -0.01$ rad (-0.57 deg).

(c) attitude, $z_l(t=0) = 0.05$ m.

(d) vertical displacement, $z_l(t=0) = 0.05$ m.

Figure 4. Attitude θ and vertical displacement z of helicopter and load, produced by a simulation run of system (10), with data from Table 1 for two different initial conditions and the other initial values equal to zero.

The 2.46 Hz natural mode is the type of anti-phase pitch oscillation which was encountered by helicopter and load during the flight. One can see that the calculated value of this undamped natural frequency is reasonably in agreement with the experienced pitch oscillation frequency, which we determined in the preceding section: 2.23 Hz and 2.35 Hz for the motion inside and outside the helicopter, respectively. When we assume that the two-legged sling was somewhat less stiff compared to the extension strop, so the value of k is somewhat lower, we find e.g. for $k_f = k_a = 1.05 \times 10^6$ N/m the natural frequency of the pitching motion at 2.30 Hz.

It is noted that this specific open tower had natural pitch and vertical bounce frequencies near 3.75 Hz, corresponding to the 1/rev frequency of the rotor system of the helicopter. Furthermore the long and relatively wide (3.4 m) load is in the hover or low-speed regime easily excited by the downwash. This interaction could be especially strong when the tip vortices of the rotor blades interact with the ends of the long load, as sketched in Fig. 5(a). The flight was at a slow airspeed, less than 40 kts, and with a heavy load, so with strong downwash, which thus remained near the helicopter at a relatively small angle of

deflection relative to the vertical. When such an aerodynamic force is excited on an end

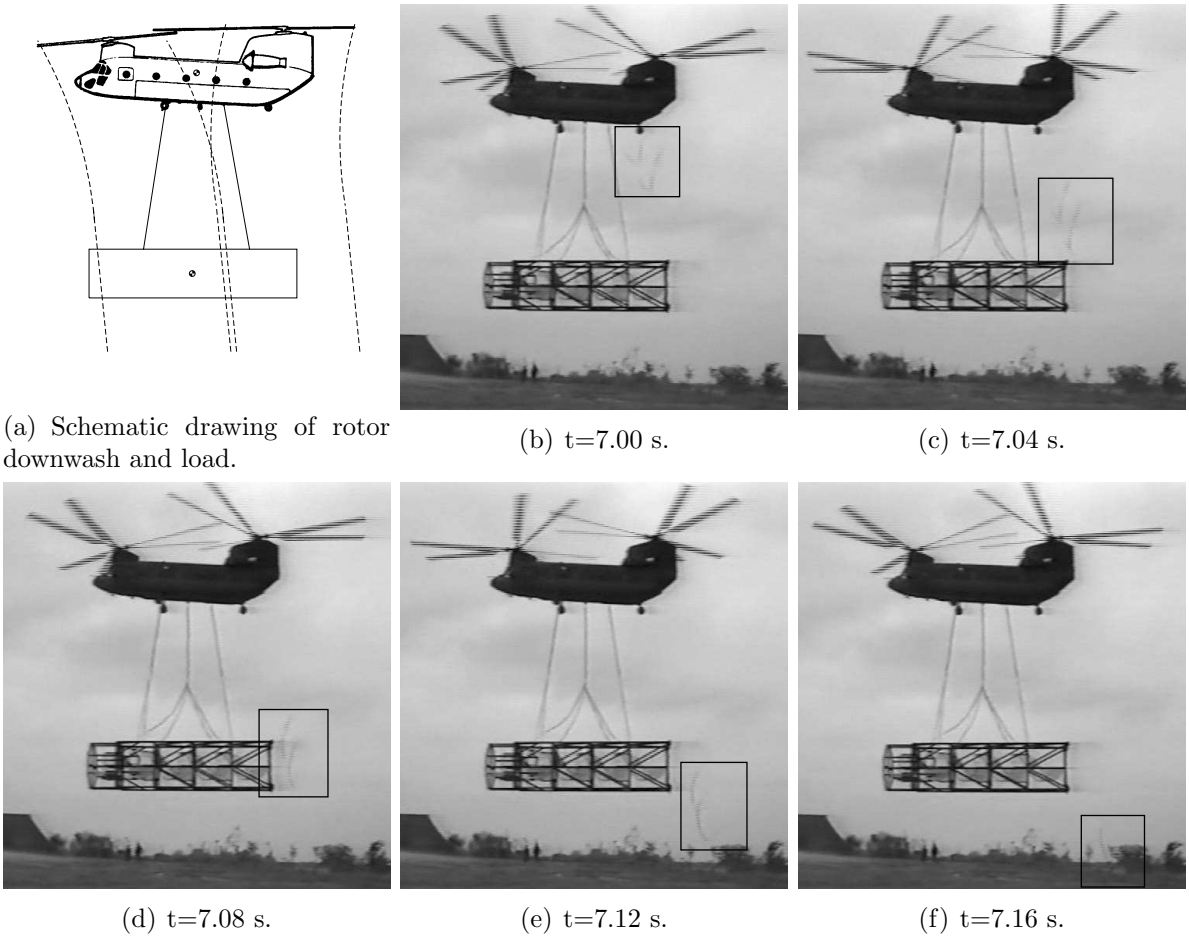

(a) Schematic drawing of rotor downwash and load.

(b) t=7.00 s.

(c) t=7.04 s.

(d) t=7.08 s.

(e) t=7.12 s.

(f) t=7.16 s.

Figure 5. Tip vortex motion.

of the load, it works with a large leverage and can thus produce a large exciting moment initiating the pitch oscillation of the relatively long load. During the analysis of the video images it was found by coincidence that a part of the tip vortex of the aft rotor became visible as a result of the high humidity. In Fig. 5, five subsequent images are shown where the condensation (indicated by the inserted rectangular box) in a part of the tip vortex of the aft rotor can be seen passing aft of the load. It is hypothesized that the close relation to the rotor 1/rev frequency might not be the only reason of the load being easily excited and poorly damped, but that the intersection of the tip vortex with the end of the load could very well have been contributing to the excitation of the resonant condition of the helicopter-load system.

4. INFLUENCE OF SLING STIFFNESS AND MASS MOMENT OF INERTIA OF THE LOAD

As we have the linearized equations of motion, Eqs. (8) or (10), we can now easily investigate the influence of a different stiffness of the slings or a different mass moment of inertia of the load. The results are plotted in Fig. 6, with f_{vb} the vertical bounce natural frequency and f_{pb} the pitch bounce natural frequency.

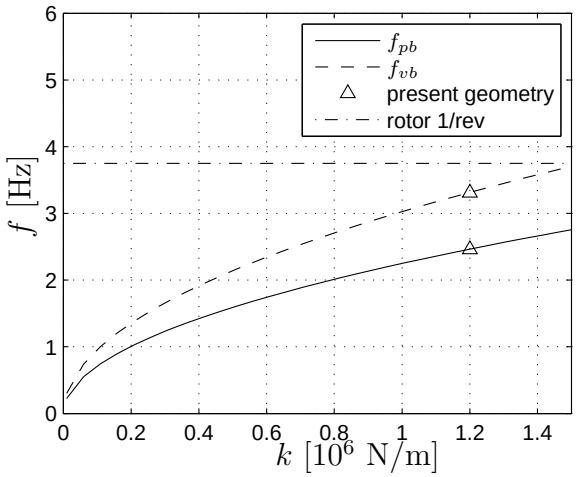

(a) Variation of the cable stiffness.

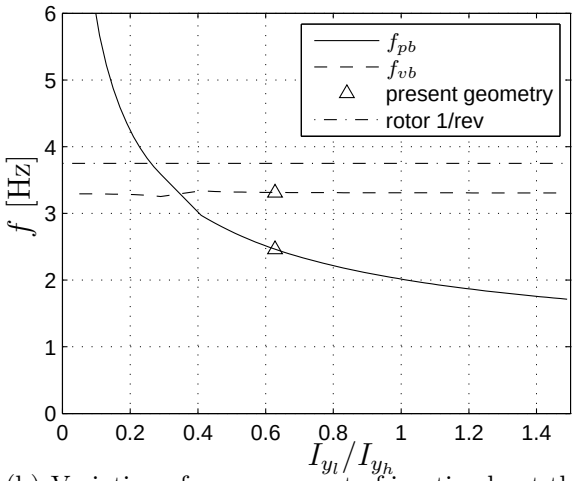

(b) Variation of mass moment of inertia about the pitch axis of the load I_{y_l}.

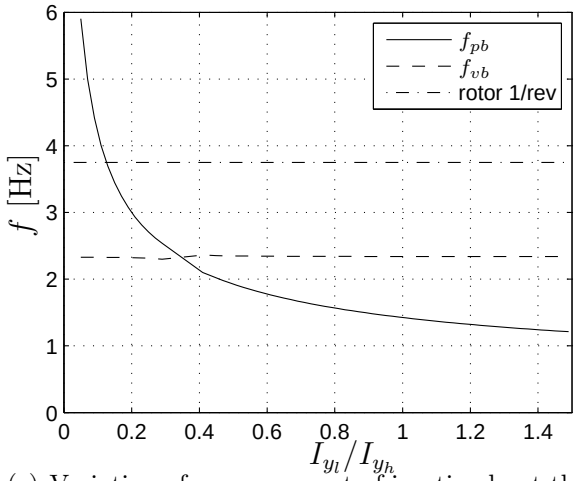

(c) Variation of mass moment of inertia about the pitch axis of the load I_{y_l}, at half spring constant.

Figure 6. Natural frequencies with variation of cable stiffness and mass moment of inertia of the load.

It is noted from Fig. 6(a) that the sling stiffness has a major influence on the natural frequencies of both the vertical and pitch bounce motion. This is important as the cable stiffness can be varied over a large range by choosing material and cable length. From Fig. 6(b) it is concluded that the influence of the mass moment of inertia of the load I_{y_l} is also relevant, but only to the pitch bounce natural frequency. This might particularly be relevant if for a certain load the mass could be distributed in different ways.

The crossing of the frequencies in Fig. 6(b) is a special point. At this value of $I_{y_l}/I_{y_h} \approx 0.340$ there is strong interaction between the two vibration modes. This is shown in Fig. 7, which is the output of system (10) for the same conditions of Fig. 4, but now for $I_{y_l}/I_{y_h} = 0.340$ with the same I_{y_h}. Comparing Fig. 7 for $I_{y_l} = 0.340 I_{y_h}$ with Fig. 4 for $I_{y_l} = 0.628 I_{y_h}$ it can be seen that the influence between both modes is greatly increased. When we change the sling stiffness, keeping the relation $k_a = k_f$, it can be seen from Eqs. (10) and (11) that the cross-over point of the two eigenfrequencies remains at the same value of I_{y_l}/I_{y_h}=0.340, which is verified by comparing Figs. 6(b) and 6(c).

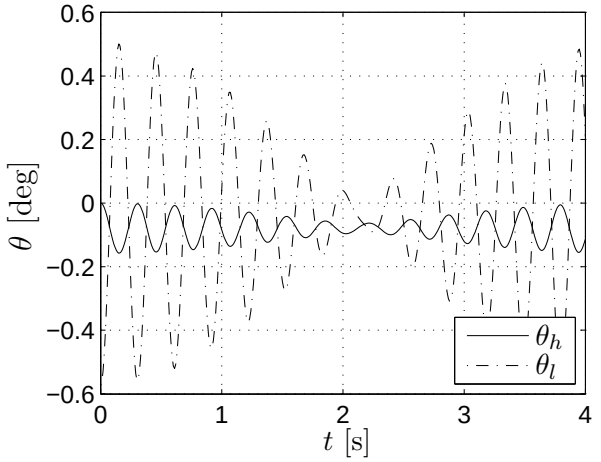

(a) attitude, $\theta_l(t=0) = -0.01$ rad (-0.57 deg).

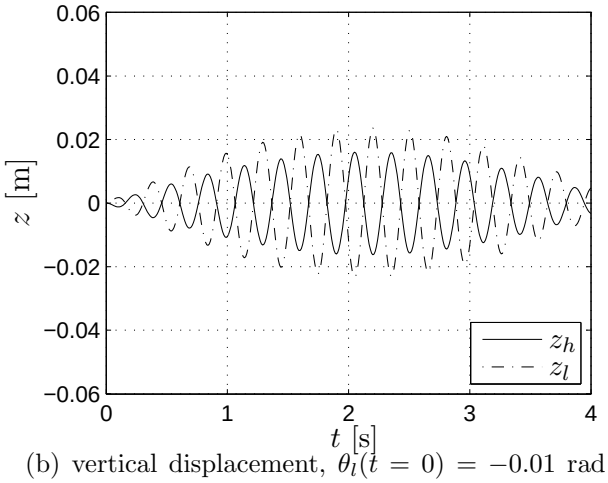

(b) vertical displacement, $\theta_l(t=0) = -0.01$ rad (-0.57 deg).

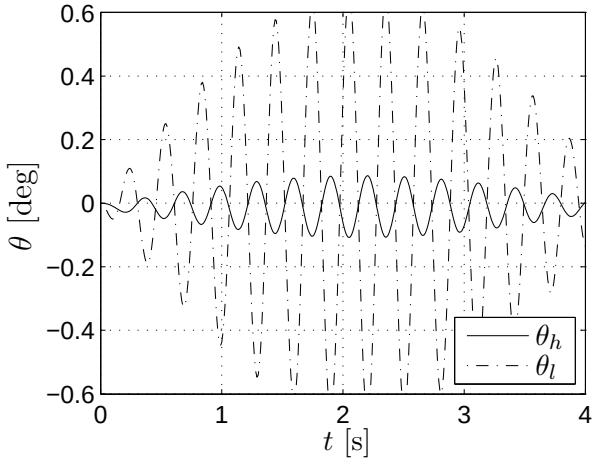

(c) attitude, $z_l(t=0) = 0.05$ m.

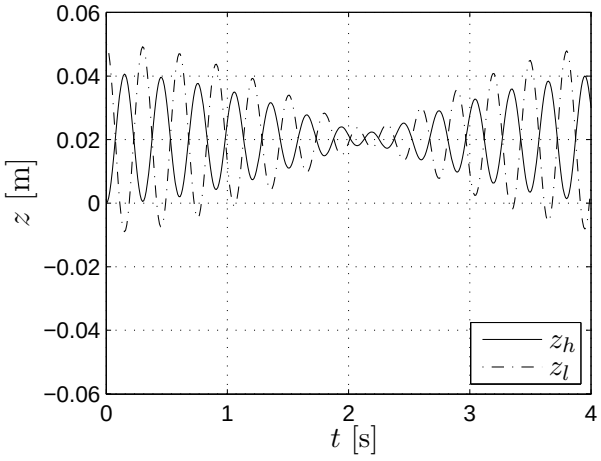

(d) vertical displacement, $z_l(t=0) = 0.05$ m.

Figure 7. Attitude and vertical displacement of helicopter and load, produced by a simulation run of system (10), with data from Table 1, except $I_{y_l} = 0.340 I_{y_h}$, *for two different initial conditions and the other initial values equal to zero.*

5. CONCLUDING REMARKS

The paper investigated the causes of a violent pitch oscillation experienced with a Chinook helicopter with a long and heavy tandem-suspended underslung load. The vibration is in agreement with the estimated motion of a 4-DOF model of helicopter and load. It seems most likely that the natural pitch bounce frequency of the system was excited during that flight. Especially as the motion did not actually diverge, but was repeatedly excited during the flight, it is hypothesized that the rotor downwash may have been contributing to the excitation of the natural pitch bounce vibration mode. In the case of the vertical bounce divergence through coupling through the pilot's arm as described by Gabel & Wilson [2], the oscilations might lead to divergent oscillations. Divergence did not occur in this case, but in some instants of persistance of the motion during the flight, the coupling through the controls might also have been a factor.

A solution to eliminate the easy excitation of the natural pitch bounce frequency, would be to decrease this natural frequency by using a lower cable stiffness in order to keep

this frequency further away of the rotor 1/rev frequency. Such a reduction of stiffness could most easily be accomplished by using extra extension strops, and thus making the cables longer. This would also result in a larger distance from the load to helicopter, and consequently in a decrease of the excitation force by the rotor downwash.

Finally, an interesting feature is the exchange of vibration modes at I_{y_l}/I_{y_h}=0.340. At this condition the energy of the vibration in z direction (vertical bounce) easily transfers to the rotation vibration in θ direction (pitch bounce) and vice versa. In this case the rotation mode can arise more easily as a result of excitation of the translational mode. The rotation vibration is more easily sensed on the pilot's station, as the pilot's station is on the end of the rotating long helicopter.

We are grateful to dr. Theo Hupkens for his great help with the data processing of the video recording.

References

[1] C. Chen, K. Y. Lim, and C. S. P. Seah. Modeling and dynamic analysis of helicopter underslung system. Number AIAA-98-4358, pages 214–224. AIAA, 1998.

[2] R. Gabel and G. J. Wilson. Test approaches to external sling load instabilities. *Journal of the American Helicopter Society*, 13(3):44–54, July 1968.

[3] A. Prabhakar. Stability of a helicopter carrying an underslung load. *Vertica*, 2:121–143, 1978.

[4] D. F. Sheldon. An appreciation of the dynamic problems associated with the external transportation of loads from a helicopter-state of the art. *Vertica*, 1:281–290, 1977.